Vegetal Melanin-induced radiative recombination centers in porous silicon

A. Benitez-Lara[1], Eduardo Coutino-Gonzalez[2,3], F. Morales-Morales[2], Mario Alberto Ávila-Gutiérrez[2], J. Carrillo-Lopez[4], Ana L. Hernández-Orihuela[5] and Agustino Martínez Antonio[6]

1 CONACYT-CIO, A.C., Loma del Bosque 115, Colonia Lomas del Campestre León, Guanajuato, México. 37150.

2 Centro de investigaciones en Óptica, A.C., Loma del Bosque 115, Colonia Lomas del Campestre León, Guanajuato, México. 37150.

3 Sustainable Materials Unit VITO, Flemish Institute for Technological Research Boeretang, 200, B-2400, Belgium.

4 CIDS-IC, Benemérita Universidad Autónoma de Puebla, Ed. IC5, Colonia San Manuel, Puebla 72570, México.

5 Evogenia, 5 de Mayo 517, Irapuato 36500, México.

6 Laboratorio de Ingeniería Biológica, Departamento de Ingeniería Genética, Centro de Investigación y de Estudios Avanzados del IPN-Unidad Irapuato, Irapuato 36824, México

Abstract

Melanin has attracted significant attention in recent years due to its optoelectronic properties exploited in micro and nano-bioelectronic applications. Herein, were report on the photoluminescence tuning of porous silicon (PSi) functionalized with melanin. PSi was prepared through an electrochemical etching process applying a density current of 2.8 mA/cm^2 to a silicon wafer using an electrolyte composed of HF and ethanol (1:1). The melanin/PSi heterojunction interface was created by drop casting a melanin solution (0.1 mg/mL in dimethyl sulfoxide) using different volumes of 10, 30 and 50 µl onto a PSi wafer. A remarkable increment of the photoluminescence intensity in the melanin/PSi interface as compared to the pristine PSi was observed through steady-state experiments. Moreover, a pronounced blue-shift (50 nm) of pristine PSi emission maximum as compared to melanin/PSi interfaces was also recorded. This behavior could be ascribed to the generation of radiative recombination centers as indicated by an increment of silicon-hydrogen (Si-H) and silicon-oxygen (Si-O) defects formed in the PSi upon interaction with the melanin, as proven by infrared (FT-IR) experiments. Time-resolved experiments revealed a remarkable decrease in the decay times of the melanin/PSi composites moving from microsecond-time components in the pristine PSi towards nanosecond decay times when the highest amount of melanin was employed; indicative of an increment of radiative recombination centers. Surface morphology changes of the composites were monitored by scanning electron microscopy (SEM), displaying the formation of small grains of melanin on the surface of the PSi up to the appearance of a melanin thin film when low and high amounts of melanin were used, respectively. This study demonstrates the enormous potential of melanin-PSi heterojunctions to provide a novel and sustainable solution for developing (bio)optoelectronic devices.

Introduction

Melanin is a ubiquitously biological pigment found in nature that has recently emerged as a very attractive material due its optoelectronic properties, such as in UV-Vis light absorption, mixed electronic-ionic conductivity and hydration state-dependent electrical conductivity. Melanin absorption can lead to the generation of heat, fluorescence, or even degradation in chemical structures due its redox properties [1-3]. Besides, melanin can be deposited in thin films to enhance its processability with microelectronic technologies displaying good adherence and uniform surface properties. Recently, eumelanin biopolymers have also been proposed for optoelectronic and photovoltaic applications using its light spectrum absorption and electronic properties [3-5]. The molecular structure of melanin is still complex to resolve and not yet fully understood but the basic compounds are 5,6-dihydroxyindol (DHI) and 2-carboxylated form 5,6-dihydroxyindole-2-carboxylic acid (DHICA) [2,6,7]. Insolubility in water, a broad pH range and irregular of constituent subunits are some characteristics of the melanin which implies that melanin is soluble in certain solvents, acids and bases such as DMSO, sulphuric acid and sodium hydroxide [1]. Another interesting characteristic of the melanin is the chelate effect which is the affinity to bond with metallic ions. On the other hand, porous silicon (PSi) is a semiconductor material compatible with microelectronic technology for the fabrication of heterojunction devices. Particularly, PSi films have attracted the semiconductor industry attention due to its wide luminescence spectra at room temperature making PSi a potential candidate for the fabrication of optoelectronic devices. The porous structure of the PSi increases the effective area and can be filled with UV absorbing biopolymer to passivate the Psi surface for applications in biosensing [8-11]. Also, PSi is considered as biocompatible and displays a tuneable luminescence response that could be modulated during the synthesis process [12-16]. The origin of PSi luminescence has been postulated as a combination of Si-quantum dots (Si-QDs) and luminescent defects (related to SiO_{2-x}) spanning from red emission to shorter wavelengths [17-21].

Melanin and PSi have been studied as heterojunctions for solar cell applications [8, 22-23]. Dmytro and collaborators use the eumelanin and the PSi obtained by metal-assisted chemical etching with Au, Cu and Ag nanoparticles. This report focused on the electrical characterization of the PSi-melanin heterojunction with an increment of the photocurrent generation, showing that the combination of the luminescence properties of PSi and the electrical, optical and redox properties of the melanin could be used to produce optoelectronic devices such as photodetectors or solar cells with a wide range of spectral responses. Here, we report on the shifting and increment of the PSi luminescence by adding melanin in different amounts onto PSi films and monitoring the photoluminescence response to identify the emission contributions which were later studied by their vibrational modes determined by FT-IR. According to these results, the lifetime carrier is shortened with the increment of the radiative recombination centers and correlated with the

infrared results [24-26]. Then, SEM micrographs morphology reveals the distribution of the Melanin on the Psi like thin film and agglomerates with respect to the amount. Therefore, this study lays the groundwork to contribute with the evolution of novel optoelectronic devices based on organic/inorganic materials heterojunctions.

Experimental Setup

PSi substrate was formed by an electrochemical etching process of a (100) p type silicon wafer with a resistivity from 1 - 10 Ω − cm. Prior to the etching process, the wafer was subject to a RCA standard cleaning process followed by immersing the Si-wafer in a 10% hydrofluoric acid (HF) solution to remove the native oxide. The electrochemical etching process was carried out inside of a 3D-printed reactor designed to control the exposure area of the wafer to 15 mm of diameter. The chemical reaction was triggered by exposing the Si-wafer to an electrolyte solution composed of a diluted hydrofluoric acid (HF) at 48% and ethanol at 99.9% in a volumetric ratio of 1:1. In this sense, the Si-wafer was etched with an active area of 1.76 cm^2 applying a current of 5 mA for 20 min using a Keithley source unit model 2450.

Melanin was dissolved with dimethyl sulfoxide (DMSO) in a concentration of 0.1mg/ml by mechanical stirring. The melanin was provided by Evogenia (batch Fbme21-03). To create the heterojunction, a drop-casting technique was employed to deposit the melanin onto the PSi using a temperature of 90 °C to evaporate the solvent during 10 minutes by dropping 5 µl of the melanin solution until the desired amount was reached. Three deposits of melanin were conducted at 10, 30 and 50 µl of volume on PSi leaving one pristine PSi sample as a reference.

Characterizations of the films were performed via FT-IR, photoluminescence (PL) spectroscopy, scanning electron microscopy (SEM) and microsecond time-resolved measurements. The FTIR spectra were measured with an Angilent Cary model 670 in ATR mode. PL was conducted using a 2300i spectrograph from Acton Research with a R955 Hamamatsu photomultiplier tube and an excitation wavelength of 330 nm in a measurement range of 400 to 800 nm. The nanosecond to millisecond time-resolved luminescence data were recorded using a 355 nm laser pulse (10 ns, 10 Hz) generated by a system consisting of a pulsed Nd:YAG laser (Quanta-Ray INDI-40, Spectra Physics) to excite the samples. The micrographs were obtained with a JEOL field emission SEM model JSM-7800F.

Results

FTIR of the PSi samples with melanin are shown in Figure 1. The melanin contributes with the increment of luminescent recombination centers through bondings with silicon and the aromatic rings. In other words, bonds between silicon and the elements from the melanin such as carbon, oxygen, and hydrogen are created. The principal FTIR peaks from the region of 600 - 1300 cm^{-1} are shown in Figure 1a. The peak of 618 cm^{-1} corresponds to Si-Si phonon modes. However, the peaks

at 834, 1048 and 1134 cm^{-1} are correlated with Si-O bending, Si-O stretching and Si-O stretching out of phase, respectively [24-28]. The interaction between PSi and melanin are attributed to the 790 and 943 cm^{-1} peaks which are not present in the PSi FT-IR spectrum with an increment related to the deposition of the melanin. In contrast, the region at 1400 to 3000 cm^{-1} in Figure 1b does not show many differences among the samples [29-33, 35]. The Si-H bonds are associated with 1972, 2034 and 2257 cm^{-1} which are created during the etching process for obtaining the PSi [27]. Bands at 1606 and 2881 cm^{-1} are attributed to the C=C and C=O bonds from the melanin, table 1 displays a compilation of the FTIR bonds observed in the different samples [27, 32, 33]. It´s well known that Ramman spectroscopy is a complement to FTIR. However, for this case we did not consider because the analysis of the band in each spectra is complex due the dependence with the structural arrangement of the melanin, its biochemical environment, amplitude and the position of the bands could change [34]. A theoretical model to explain the bonds between Melanin and Silicon was proposed by A. Antidormi. This reference describes the bonds created when the melanin is deposited on silicon substrates which support the FTIR results and the Eg behavior [35].

Measurements of PL are shown in Figure 2 with an increment of the intensity due to PSi/melanin interaction. The PL emission is based by the band theory. An electron absorbs the photon energy and makes a transition from the valence band to the conduction band. After, the electron get backs to the valence band and the electron releases the energy absorbed in photons form. Between the Band gap appear tramps which are correlated to defects, excitons or open bonds. So in this case, the radiative defects are tramps created into the band gap by the passivation at the interface of the PSi/melanin with a tendency with respect to the deposition of the melanin. It is well known that the melanin under UV radiation has an oxidation reduction process where melanin moieties undergo changes allowing an electronic or ionic interchange with the PSi, creating radiative recombination. In this sense, the shifting of the emission is correlated with defects. In general, the emission of the PSi has been ascribed to the quantum confinement (QC) and surface defects [36-41]. The emission from the 700 to 800 nm is associated with the QC and some dangling bonds, however, the defects emission predominate in the range from 525 to 700 nm. The quantum confinement is present in the Silicon nanocrystals embedded into the porous silicon structure. The model of this process is presented in equation 1 which is based in the approximation of the effective mass that predicts the dependence of effective band-gap with the particle size. Where m_h^*, m_e^* are the effective mass of holes and electron, respectively and L_x^2, L_y^2 and L_z^2 corresponds to the dimensions of the nanoparticles. The band gap of bulk silicon is denoted by Eg and for the silicon nanoparticle is ESi-np. The quantum confinement occurs when the nanoparticles are around of Bohr´s radio (~ 5 nm) starting emission from 700 nm. The emission of the QC could be explained by the radiative recombination band to band from the electron-holes confined in silicon nanocrystals [42].

$$E_{Si-np} = E_g + \left(\frac{1}{L_x^2} + \frac{1}{L_y^2} + \frac{1}{L_z^2}\right) + \left(\frac{1}{m_e^*} + \frac{1}{m_h^*}\right)\frac{\hbar^2\pi^2}{2} \quad (1)$$

Other emission mechanisms have been associated to the radiative centers created during the etching process. Upon completion of the etching process, the silicon oxidizes instantly during

drying, growing a thin film of SiO_2 on the PSi surface. The radiative recombination centers are located in the SiO_2 /PSi interface such as neutral oxygen vacancy (NOV), self-trapped exciton and non-bridging oxygen hole center (NBOHC) with emission on ~520, ~580 and ~650 nm, respectively [39-41]. In this study, the contribution of the melanin in the luminescence could be related to the passivation of the PSi surface and the Redox properties during the UV excitation. The increment of the luminescent centers, with respect to the PSi sample, could be appreciated in the spectra of the samples in Figure 2a. For the samples PSi-10 µl, PSi-30 µl and PSi-50 µl the increment in luminescence is in the range of 500 to 700 nm which is correlated to the luminescent defects. FTIR and PL correlation indicates that the melanin-functionalized samples display an increment of the peaks at 790, 878, 943 and 1043 cm^{-1} which corresponds to the passivation of the sample due to the H, O and C bonds with the PSi. Our theory is the passivation occurs when the deposition of melanin is done, however, when the Melanin/PSi is under UV radiation, the melanin molecule changes creating vacancies and dangling bonds such as NBOHC [1-3, 42]. The increment of recombination centers reduces the carrier lifetime which could be appreciated in Figure 2b. The lifetime carriers at 720 nm shows a tendency with the increment of melanin, resulting in reduction of the lifetime compared with the pristine PSi. The decay times for the sample PSi-50 µl were not measured due to its very fast nature (nanoseconds time-frame) falling out of the detection limit of the technique (10 ns), probably due to molecular transitions by the melanin self.

The measurement of absorbance was made in a range of 300 to 800 nm shown in figure 3. The absorption of the PSi is higher than the Melanin. However, the absorption of the Melanin/PSi samples increase in the visible range. Though, there is absorption in the visible range from 400 to 700 nm for Melanin/PSi samples where the absorption increases with the thickness of the melanin films and affect the PL emission such as the PSi50µl sample. In other way, the absorption in the range between 300 to 400 nm decreases for the samples PSi10µl and PSi30µl, but increases for the PSi50µl which is correlated with the increment of the recombination centers, which is congruent with the PL and FTIR results.

Drop casting was the method to deposit the melanin solution where the deposits were of 5 µl reaching dry and adding another drop to obtain three different amounts, 10, 30 and 50 µl. When the DMSO evaporates certain melanin regions did not distribute homogeneously on the surface, but adding another drop of the solution, the dry melanin is redistributed over the PSi. For the case of PSi-10µl, the deposition of the melanin is non-homogeneous with some agglomerates like particles and thin film covering the PSi (Figure 3b). However, the PSi-30µl sample has a homogeneous distribution over the PSi compared with the PSi-10µl sample, covering a bigger area, with thickness of around 30 nm as displayed in Figure 3c. The sample of Psi-50µl shows an agglomeration over the surface of the PSi by the excess of melanin, creating shadows that absorb UV radiation which does not reach the PSi as shown in the PL results.

Conclusion

The melanin redox properties are sufficient to passivate the PSi, creating luminescent recombination centers whit a shift and increment in the PL response. According to PL emission,

the defect with highest changes is the NBOHC (around 630 nm) which is correlated with the increment of FTIR peak in 834, 878 and 943 cm^{-1} that is associated with bonds between Si-O and Si-C. These bonds are created by the modification of the molecule by the UV radiation. The carrier timelife reduces in each sample with the increment of melanin; this heterojunction could be applied to build optoelectronic devices with fast response in the UV region. The morphology of the deposited melanin changes with each drop of the solution added to the PSi. For an area of 1.7 cm^2 of PSi, 30 µl of melanin solution has good homogeneity, demonstrating that DMSO is an adequate solvent to deposit the melanin in thin films and introduce it into the porous silicon structure.

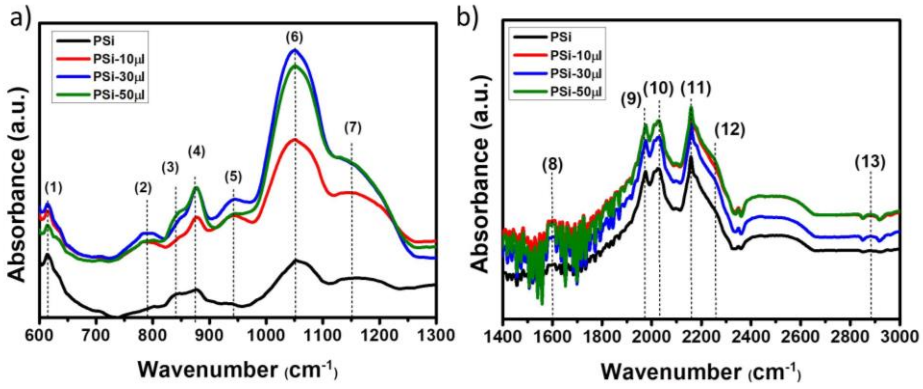

Figure 1 FTIR spectra from the samples of PSi/melanin in the range of a) 600 to 1300 and b) 1400 to 3000 cm^{-1}.

Table 1 FTIR absorption peaks showing vibrational modes of bonds between the PSi and melanin interface labeled in figure1.

	Position (cm^{-1})	Material	Assignment	Reference
(1)	618	PSi	Si-Si	[24, 25].
(2)	790	PSi-Melanin	Aromatic ring (AR) and CH_3 on Psi	[29, 27, 230]
(3)	834	PSi	Si-O bending	[26]

(4)	878	PSi	Si-H or Si_2-O_3	[26]
(5)	943	PSi-Melanin	Si-C Stretching	[26, 41]
(6)	1048	PSi	Si-O Stretching	[24]
(7)	1134	PSi	Si-O Stretching out of phase	[24]
(8)	1604	Melanin/PSi	C=O or C=C Stretching	[29, 30, 32]
(9)	1972	PSi	Si-H	[25, 27]
(10)	2034	PSi	Si-H	[27]
(11)	2157	Psi/Melanin	C_2Si-H_2, CH_3CSi-H and CSi-H_3	[25]
(12)	2257	PSi	Si-H stretching	[33, 26]
(13)	2881	Melanin	C-H stretching	[32, 36, 27]

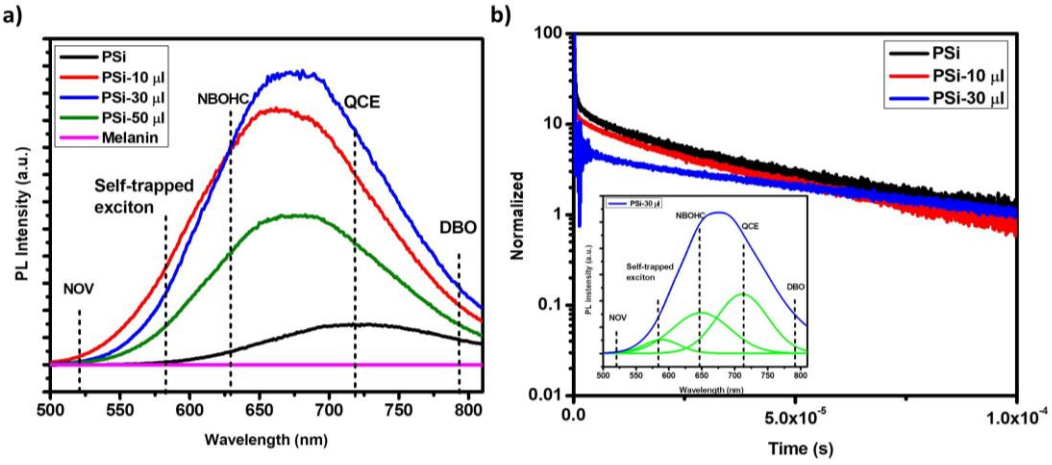

Figure 2 Photoluminescence from the PSi with melanin. a) An increase of luminescence is appreciated within the range of 500 to 650 nm corresponding to emission defects. b) Lifetime decay times decrease with the increment of radiative recombination centers.

Table 2 PL emissions defects from the melanin/PSi interface. According to FTIR, the increment of the emission defects is correlated to the bonds of oxygen and carbon with silicon favored by the melanin.

Emision (nm)	Energy (eV)	Material	Method PL	REF.
520	2.4	SiOx	The NOV defect.	[38]
580	2.1	SiOx	Self-trapped exciton	[39, 40]
630	1.96	SiOx	NBOHC (Non-Bridging Oxygen Hole Center).	[39-45]
720	1.7	SiOx	QCE (Quantum confinement effects).	[20, 45]

790	1.56	SiOx	Dangling bonds and oxygen-related defects.	[42]

215

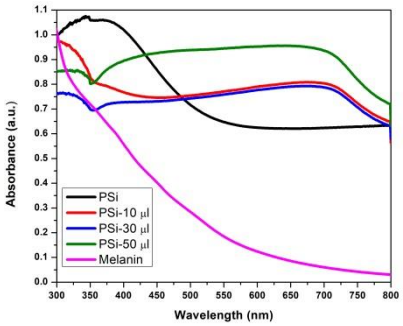

Figure 3 Absorbance spectra. The absorption gets a broadband due combination of the melanin and PSi properties. In the visible range, the absorption increase due the amount of the melanin over the PSi.

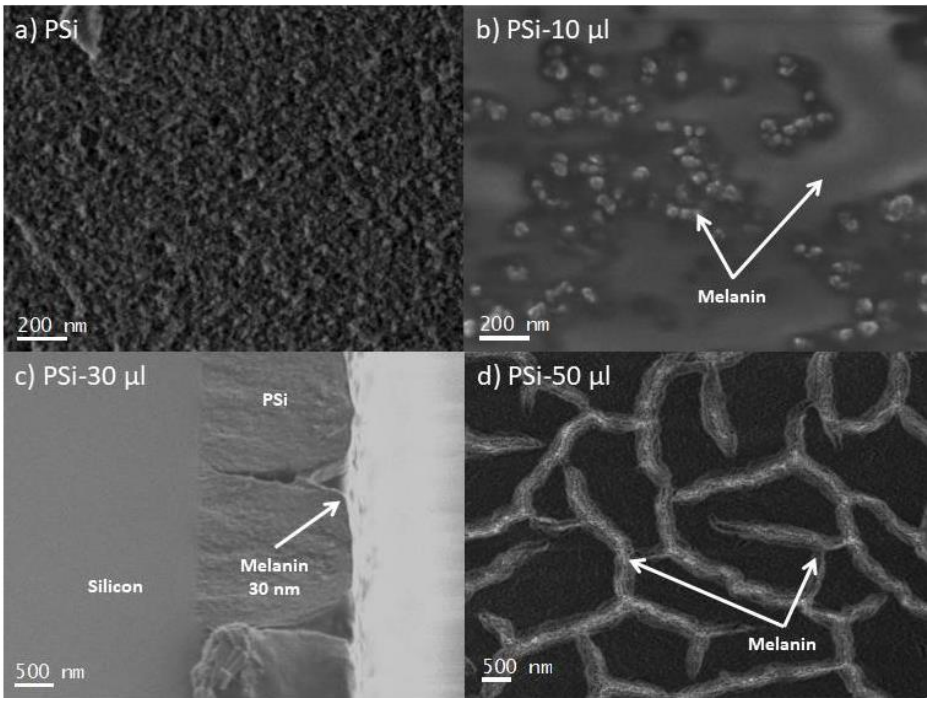

220

Figure 4 Micrographs of the samples of PSi with melanin. a) Pristine PSi. b) PSi with 10 µl of melanin, where agglomerates and a thin film is observed. c) PSi with 30 µl of melanin showing the thin film without agglomerates and 30 nm of thickness. d) PSi with 50 µl of melanin with agglomerates over the PSi.

References

[1] E. Vahidzadeh, A.P. Kalra, K. Shankar, Melanin-based electronics: From proton conductors to photovoltaics and beyond, Biosens. Bioelectron. 122 (2018) 127–139. https://doi.org/10.1016/j.bios.2018.09.026.

[2] M. Xiao, M.D. Shawkey, A. Dhinojwala, Bioinspired Melanin-Based Optically Active Materials, Adv. Opt. Mater. 8 (2020) 1–15. https://doi.org/10.1002/adom.202000932.

[3] E. Shembel, V. Kyrychenko, I. Maksyuta, V. Redko, N. Zaderey, Melanin as Semiconductor with Polymer Structure is Effective Modifier for Electrodes of High-Energy Li-Ion Batteries, ECS Trans. 99 (2020) 47–55. https://doi.org/10.1149/09901.0047ecst.

[4] C.A. Canaria, I.N. Lees, A.W. Wun, G.M. Miskelly, M.J. Sailor, Characterization of the carbon-silicon stretch in methylated porous silicon-observation of an anomalous isotope shift in the FTIR spectrum, Inorg. Chem. Commun. 5 (2002) 560-564.

[5] E. Vahidzadeh, A.P. Kalra, K. Shankar, Melanin-based electronics: From proton conductors to photovoltaics and beyond, Biosens. Bioelectron. 122 (2018) 127–139. https://doi.org/10.1016/j.bios.2018.09.026.

[6] N. Madkhali, H.R. Alqahtani, S. Alterary, H.A. Albrithen, A. Laref, A. Hassib, Characterization and electrochemical deposition of natural melanin thin films, Arab. J. Chem. 13 (2020) 4987–4993. https://doi.org/10.1016/j.arabjc.2020.01.021.

[7] M. D'Ischia, A. Napolitano, A. Pezzella, P. Meredith, T. Sarna, Chemical and structural diversity in eumelanins: Unexplored bio-optoelectronic materials, Angew. Chemie - Int. Ed. 48 (2009) 3914–3921. https://doi.org/10.1002/anie.200803786.

[8] D. Volynskyi, M. Dusheiko, R. Madan, N. Kutuzov, T. Obukhova, Melanin/porous silicon heterojunctions for solar cells and sensors applications, in: 2020 IEEE 40th Int. Conf. Electron. Nanotechnology, ELNANO 2020 - Proc., Institute of Electrical and Electronics Engineers Inc., 2020: pp. 343–346. https://doi.org/10.1109/ELNANO50318.2020.9088805.

[9] L. De Stefano, S. D'Auria, Confocal imaging of protein distributions in porous silicon optical structures, J. Phys. Condens. Matter. 19 (2007). https://doi.org/10.1088/0953-8984/19/39/395009.

[10] L. De Stefano, M. Rossi, M. Staiano, G. Mamone, A. Parracino, L. Rotiroti, I. Rendina, M. Rossi, S. D'Auria, Glutamine-binding protein from Escherichia coli specifically binds a wheat gliadin peptide allowing the design of a new porous silicon-based optical biosensor, J. Proteome Res. 5 (2006) 1241–1245. https://doi.org/10.1021/pr0600226.

[11] L. De Stefano, I. Rea, P. Giardina, A. Armenante, I. Rendina, Protein-modified porous silicon nanostructures, Adv. Mater. 20 (2008) 1529–1533. https://doi.org/10.1002/adma.200702454.

[12] C.H. Lin, S.C. Lee, Y.F. Chen, Strong room-temperature photoluminescence of hydrogenated amorphous silicon oxide and its correlation to porous silicon, Appl. Phys. Lett. 63 (1993) 902–904. https://doi.org/10.1063/1.109867.

[13] S. Ye, F. Xiao, Y.X. Pan, Y.Y. Ma, Q.Y. Zhang, Phosphors in phosphor-converted white light-emitting diodes: Recent advances in materials, techniques and properties, Mater. Sci. Eng. R Reports. 71 (2010) 1–34. https://doi.org/10.1016/j.mser.2010.07.001.

[14] V. Myndrul, R. Viter, M. Savchuk, N. Shpyrka, D. Erts, D. Jevdokimovs, V. Silamiķelis, V. Smyntyna, A. Ramanavicius, I. Iatsunskyi, Porous silicon based photoluminescence immunosensor for rapid and highly-sensitive detection of Ochratoxin A, Biosens. Bioelectron. 102 (2018) 661–667. https://doi.org/10.1016/j.bios.2017.11.048.

[15] T. Nikitin, L. Khriachtchev, Optical and structural properties of si nanocrystals in SiO2 films, Nanomaterials. 5 (2015) 614–655. https://doi.org/10.3390/nano5020614.

[16] F. Karbassian, Porous Silicon, Porosity - Process. Technol. Appl. (2018) 3–36. https://doi.org/10.5772/intechopen.72910.

[17] V. Lehmann, U. Gösele, Porous silicon formation: A quantum wire effect, Appl. Phys. Lett. 58 (1991) 856–858. https://doi.org/10.1063/1.104512.

[18] T.L.S.L. Wijesinghe, E.J. Teo, D.J. Blackwood, Potentiostatic formation of porous silicon in dilute HF: Evidence that nanocrystal size is not restricted by quantum confinement, Electrochim. Acta. 53 (2008) 4381–4386. https://doi.org/10.1016/j.electacta.2008.01.057.

[19] F. Morales-Morales, L. Palacios-Huerta, S.A. Cabañas-Tay, A. Coyopol, A. Morales-Sánchez, Luminescent Si quantum dots in flexible and semitransparent membranes for photon down converting material, Opt. Mater. (Amst). 90 (2019) 220–226. https://doi.org/10.1016/j.optmat.2019.02.043.

[20] F. Morales-Morales, A. Benítez-Lara, N. Hernández-Sebastián, F. Ambriz-Vargas, M.R. Jiménez-Vivanco, R. López, A. Morales-Sánchez, Study of zinc oxide/porous silicon interface for optoelectronic devices, Mater. Sci. Semicond. Process. 148 (2022). https://doi.org/10.1016/j.mssp.2022.106810.

[21] L. Skuja, The origin of the intrinsic 1.9 eV luminescence band in glassy SiO2, J. Non. Cryst. Solids. 179 (1994) 51–69.https://doi.org/10.1016/0022-3093(94)90684-X.

[22] G. Mula, L. Manca, S. Setzu, A. Pezzella, Photovoltaic properties of PSi impregnated with eumelanin, 2012.http://www.nanoscalereslett.com/content/7/1/377.

[23] E. Vahidzadeh, A.P. Kalra, K. Shankar, Melanin-based electronics: From proton conductors to photovoltaics and beyond, Biosens. Bioelectron. 122 (2018) 127–139. https://doi.org/10.1016/j.bios.2018.09.026.

[24] J. Divkovic Puksec, Recombination Processes and Holes and Electrons Lifetimes, Automatika, 43 (2002) 47–53.

[25] D. Neamen, Semiconductor Physics and Devices, Mc. Graw-Hill higher education, 2003.

[26]P. Aigrain, Recombination processes in semiconductors, Nuovo Cim. Ser. 10. 7 (1958) 724–729. https://doi.org/10.1007/BF02751505.

[27] D. Liu, P. Yuan, H. Liu, J. Cai, D. Tan, H. He, J. Zhu, T. Chen, Quantitative characterization of the solid acidity of montmorillonite using combined FTIR and TPD based on the NH3 adsorption system, Appl. Clay Sci. 80–81 (2013) 407–412. https://doi.org/10.1016/j.clay.2013.07.006.

[28] F. Shariatmadar Tehrani, B.T. Goh, M.R. Muhamad, S.A. Rahman, Pressure dependent structural and optical properties of silicon carbide thin films deposited by hot wire chemical vapor deposition from pure silane and methane gases, J. Mater. Sci. Mater. Electron. 24 (2013) 1361–1368. https://doi.org/10.1007/s10854-012-0934-z.

[29] R. Hou, X. Liu, K. Xiang, L. Chen, X. Wu, W. Lin, M. Zheng, J. Fu, Characterization of the physicochemical properties and extraction optimization of natural melanin from Inonotus hispidus mushroom, Food Chem. 277 (2019) 533–542. https://doi.org/10.1016/j.foodchem.2018.11.002.

[30] S. Roy, L. Van Hai, H.C. Kim, L. Zhai, J. Kim, Preparation and characterization of synthetic melanin-like nanoparticles reinforced chitosan nanocomposite films, Carbohydr. Polym. 231 (2020) 115729. https://doi.org/10.1016/j.carbpol.2019.115729.

[31] C.A. Canaria, I.N. Lees, A.W. Wun, G.M. Miskelly, M.J. Sailor, Characterization of the carbon-silicon stretch in methylated porous silicon-observation of an anomalous isotope shift in the FTIR spectrum, n.d. www.elsevier.com/locate/inoche.

[32] F. Ay, A. Aydinli, Comparative investigation of hydrogen bonding in silicon based PECVD grown dielectrics for optical waveguides, Opt. Mater. (Amst). 26 (2004) 33–46. https://doi.org/10.1016/j.optmat.2003.12.004.

[33] K.T. Queeney, Y.J. Chabal, K. Raghavachari, Role of interdimer interactions in NH3 dissociation on Si(100)-(2 × 1), Phys. Rev. Lett. 86 (2001) 1046–1049. https://doi.org/10.1103/PhysRevLett.86.1046.

[34] B.P. Yakimov, E.A. Shirshin, J. Schleusener, A.S. Allenova, V. V. Fadeev, M.E. Darvin, Melanin distribution from the dermal–epidermal junction to the stratum corneum: non-invasive in vivo assessment by fluorescence and Raman microspectroscopy, Sci. Rep. 10 (2020) 1–13. https://doi.org/10.1038/s41598-020-71220-6.

[35] A. Antidormi, C. Melis, E. Canadell, L. Colombo, Assessing the Performance of Eumelanin/Si Interface for Photovoltaic Applications, J. Phys. Chem. C. 121 (2017) 11576–11584. https://doi.org/10.1021/acs.jpcc.7b02970.

[36] I.E. Pralea, R.C. Moldovan, A.M. Petrache, M. Ilieș, S.C. Hegheș, I. Ielciu, R. Nicoară, M. Moldovan, M. Ene, M. Radu, A. Uifălean, C.A. Iuga, From extraction to advanced analytical methods: The challenges of melanin analysis, Int. J. Mol. Sci. 20 (2019). https://doi.org/10.3390/ijms20163943.

[37] D. Comedi, O.H.Y. Zalloum, J. Wojcik, P. Mascher, Light emission from hydrogenated and unhydrogenated Si-nanocrystal/Si dioxide composites based on PECVD-grown Si-rich Si oxide films, IEEE J. Sel. Top. Quantum Electron. 12 (2006) 1561–1569. https://doi.org/10.1109/JSTQE.2006.885388.

[38] G.S. Kiran, S.A. Jackson, S. Priyadharsini, A.D.W. Dobson, J. Selvin, Synthesis of Nm-PHB (nanomelanin-polyhydroxy butyrate) nanocomposite film and its protective effect against biofilm-forming multi drug resistant Staphylococcus aureus, Sci. Rep. 7 (2017) 1–13. https://doi.org/10.1038/s41598-017-08816-y.

[39] C.J. Lin, G.R. Lin, Defect-enhanced visible electroluminescence of multi-energy silicon-implanted silicon dioxide film, IEEE J. Quantum Electron. 41 (2005) 441–447. https://doi.org/10.1109/JQE.2004.842314.

[40]S. Boggs, D. Krinsley, Application of cathodoluminescence imaging to the study of sedimentary rocks, Cambridge University Press, 2006.

[41] L. Skuja, The origin of the intrinsic 1.9 eV luminescence band in glassy SiO2, J. Non. Cryst. Solids. 179 (1994) 51–69. https://doi.org/10.1016/0022-3093(94)90684-X.

[42] T. Nikitin, L. Khriachtchev, Optical and structural properties of si nanocrystals in SiO2 films, Nanomaterials. 5 (2015) 614–655. https://doi.org/10.3390/nano5020614.

[43] O. Bisi, S. Ossicini, L. Pavesi, Porous silicon: A quantum sponge structure for silicon based optoelectronics, Surf. Sci. Rep. 38 (2000) 1–126. https://doi.org/10.1016/S0167-5729(99)00012-6.

[44] P.M. Fauchet, L. Tsybeskov, S.P. Duttagupta, K.D. Hirschman, Stable photoluminescence and electroluminescence from porous silicon, Thin Solid Films. 297 (1997) 254–260. https://doi.org/10.1016/S0040-6090(96)09438-2

[45] A. Cullis, L. Canham, Visible light emission due to quantum size effect in high porous crystalline silicion, Nature. 354 (1991) 56–58.